Check for updates

Tuning the mechanical impedance of disordered networks for impact mitigation†

Marcos A. Reyes-Martinez, [iD] [a] Edwin P. Chan, [iD] *[a] Christopher L. Soles,[a] Endao Han, [iD] [bc] Kieran A. Murphy,[c] Heinrich M. Jaeger,[bc] Daniel R. Reid[d] and Juan J. de Pablo [iD] [d]

Disordered-Network Mechanical Materials (DNMM), comprised of random arrangements of bonds and nodes, have emerged as mechanical metamaterials with the potential for achieving fine control over their mechanical properties. Recent computational studies have demonstrated this control whereby an extremely high degree of mechanical tunability can be achieved in disordered networks *via* a selective bond removal process called pruning. In this study, we experimentally demonstrate how pruning of a disordered network alters its macroscopic dynamic mechanical response and its capacity to mitigate impact. Impact studies with velocities ranging from 0.1 m s^{-1} to 1.5 m s^{-1} were performed, using a mechanical impactor and a drop tower, on 3D printed pruned and unpruned networks comprised of materials spanning a range of stiffness. High-speed videography was used to quantify the changes in Poisson's ratio for each of the network samples. Our results demonstrate that pruning is an efficient way to reduce the transmitted force and impulse from impact in the medium strain rate regime (10^1 s^{-1} to 10^2 s^{-1}). This approach provides an interesting alternative route for designing materials with tailored impact mitigating properties compared to random material removal based on open cell foams.

An impact, characterized as high force or a blast event experienced by a target over a short time, is something that should be avoided. When it is unavoidable, the severity can be reduced with an impact mitigation system. In the case of head protection, a protective structure (*e.g.* helmet) is worn over the head to protect the delicate target (*e.g.* brain).[1] Understanding the optimal structure for mitigating an impact requires one to balance the materials properties of the impact mitigation system to the conditions of a particular impact.

In the case of the helmet, it can be reduced to a one-dimensional spring-mass system (Fig. 1a) where a mass m_i impacts a protective structure of mass m_p and stiffness k_p at a velocity v_0. The parameters m_t and k_t correspond to the mass and stiffness of the target. A time-dependent force ($F(t)$) resulting from the initial impact is exerted on m_p that propagates to m_t at a rate determined by k_p and k_t. Mitigating this impact

requires reduction of the acceleration of the target and the amplitude of the transmitted force pulse.

Unfortunately, there is a transmitted force-impulse tradeoff in impact mitigation because the material properties that control these two dynamic properties follow opposite trends in most conventional materials. Mitigating the change in acceleration within a time interval ($\Delta t = t_2 - t_1$) requires a reduction in the transmitted impulse (I_t) relative to the incident impulse (I_i),

$$I_t = \int_{t_1}^{t_2} F_t(t)\mathrm{d}t \tag{1}$$

The ratio of transmitted to incident impulse can be related in terms of the ratio of the mass of the target (m_t) to the mass of the protective structure (m_p) as,[2]

$$\frac{I_t}{I_i} = \frac{2(m_t/m_p)}{(m_t/m_p) + 1} \tag{2}$$

Therefore, eqn (2) suggests that $m_p \gg m_t$ to effectively reduce the transmitted impulse.

Mitigating the transmitted force (F_t) relative to the incident force (F_i) requires control of the specific acoustic impedance (z), which is a measure of the resistance to mechanical deformation when subjected to a dynamic force. For an isotropic material,

[a] *Materials Science and Engineering Division, National Institute of Standards and Technology, Gaithersburg, MD 20899, USA. E-mail: edwin.chan@nist.gov*
[b] *James Franck Institute, The University of Chicago, Chicago, Illinois 60637, USA*
[c] *Department of Physics, The University of Chicago, Chicago, Illinois 60637, USA*
[d] *Pritzker School of Molecular Engineering, University of Chicago, Chicago, Illinois 60637, USA*
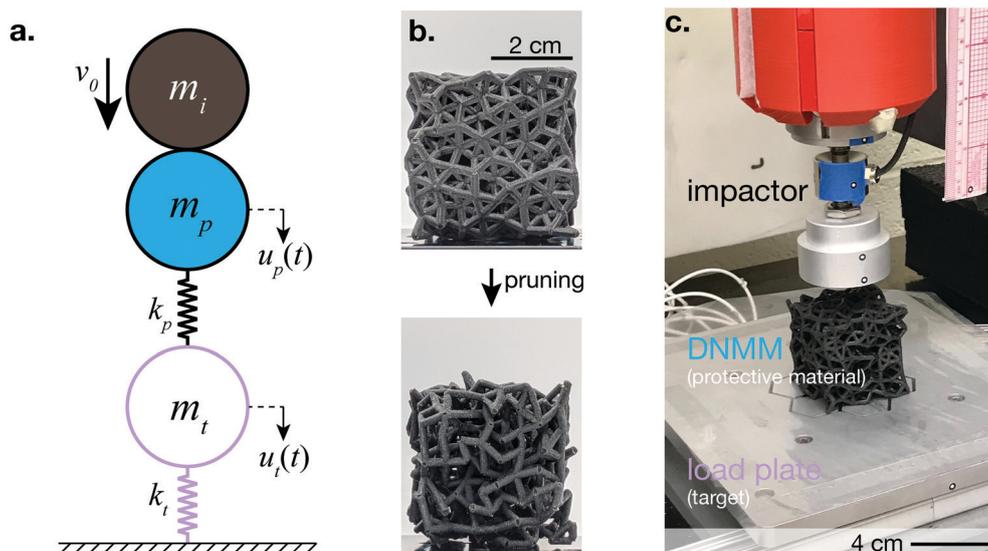† Electronic supplementary information (ESI) available. See DOI: 10.1039/d1sm01649k

Fig. 1 Impact behavior of disordered network mechanical metamaterials (DNMM). (a) An impact mitigation system represented as a one-dimensional spring-mass system. The schematic shows the time dependent force ($F(t)$), exerted by the impactor of mass m_i on the the protective material (DNMM) and target with masses m_p and m_t, respectively. The masses are coupled by springs representing the stiffnesses of the protective material and target (k_p, k_t), respectively. (b) Images of representative unpruned and pruned 3D-printed DNMM samples. (c) The drop tower experiment is composed of an instrumented drop mass, the DNMM sample and an instrumented load plate to measure the transmitted load due to impact.

this parameter is a function of the Young's modulus (E) and the mass density of the material (ρ),

$$z = \sqrt{E\rho}. \tag{3}$$

For an impact mitigating material system composed of material A layered on top of material B, the ratio of transmitted to incident force is related to the acoustic impedance of the respective materials,[3]

$$\frac{F_t}{F_i} = \frac{2z_B}{z_A + z_B} \tag{4}$$

Eqn (4) indicates that $z_B \ll z_A$ in order to reduce the transmitted force, and it is evident from eqn (3) that polymeric foams are excellent materials for impact mitigation. Their low densities and relatively low elastic constants minimize the force transmission when coupled to a second material with a higher acoustic impedance. Thus polymeric foams are widely used for impact mitigation applications ranging from the aerospace industry to footwear, personal protection and product packaging.[4-7] Although the mechanical and structural diversity of polymeric materials allows for a theoretically wide parameter space for the design of polymeric foams, actual control over these physical properties often requires radical changes in the polymerization and crosslinking chemistries, which are limited by traditional manufacturing techniques.[6,8]

There has been a recent trend towards the design and application of periodic metamaterials for impact mitigation applications.[7,9] Unfortunately, their structural symmetry limits the extent of strain or stress localization and range of tunability in extrinsic materials properties. Additionally, most of the studies on mechanical metamaterials focus on maximizing the energy absorption capacity of an impact but they have not

been designed for the specific reduction of transmitted force or impulse.[7]

An aperiodic mechanical metamaterial shows significantly different mechanical behavior. The response of each material point to a global deformation can vary drastically relative to a neighboring one.[10,11] This facilitates strain localization since bonds experiencing larger stresses are more likely to yield first. When a particular bond buckles or breaks, the changes in the global elastic constants depend on the details of the broken bond. This bond-to-bond variation in Disordered-Network Mechanical Metamaterials (DNMM) can be exploited to manipulate their mechanical properties by removal of specific bonds. The computational process that selectively removes bonds from disordered networks is known as pruning.[10,11] Compared with random bond removal, pruning allows the removal of targeted bonds that contribute the most to E for a given ρ. This control is particularly attractive in impact mitigation since the materials requirements for reducing impulse and transmitted force are different thus requiring independent optimization over the Young's modulus and density of a given material. In this work, we make advantageous use of the mechanical tunability of computationally generated DNMMs by fabricating these materials using 3D printing and then experimentally studying their mechanical response with dynamic impact experiments.

We selected a model three-dimensional disordered network and subjected it to the computational pruning process to generate a new network with a lower bulk modulus to shear modulus ratio (K/μ). Given that the seeding of the initial network is random, and the pruning algorithm will always reduce K/μ by removing the bonds that contribute the least to the global shear modulus of the network one step at a time, we expect the results from impacts experiments to be independent

of the choice of initial network. These computer generated DNMM structures were then converted to a stereolithographic file format that enables them to be realized into actual materials for impact testing (Fig. 1b). All the DNMM samples were printed using UV-curable 3D printing elastomeric resins, which offers access to a wide range of constituent materials. For this study, we focused on fabricating DNMMs using resins with Shore-A scale hardness that vary from approximately 30 (soft) to 70 (stiff). We printed all of the DNMM samples with approximate dimensions of (50 mm).[3]

To study the mechanical response of DNMMs under dynamic loading conditions, we performed instrumented dynamic impact experiments using a piston-driven mechanical impactor with impact velocities ranging from 0.1 m s^{-1} to 1.5 m s^{-1} and a drop tower with a 2.4 kg impactor mass, dropped from a height of 50 mm (Fig. 1c). The incident stress (σ_{in}) versus compressive strain (ε_{tr}) curves for unpruned DNMM and pruned DNMM printed with the Shore-A 30, 50 and 70 materials are shown in Fig. 2a, for drop mass experiments.

There is a significant drop in the stiffness of the network after pruning. This is to be expected due to the reduction in the overall load bearing ability of the network after pruning because bonds and nodes are removed in the pruning process. We also observe an apparent stiffening of the DNMMs with increasing impact velocity in mechanical impactor experiments (Fig. S1, ESI†). However, this velocity dependent stiffness does not change after the pruning process thus suggesting that this change is a property of the constituent material (*i.e.* an intrinsic property), and not a result of the change in the macroscopic structure of the network (*i.e.* an extrinsic property). We attribute the strain stiffening behavior to a combination of the viscoelastic properties[13] of the constituent materials used to 3D print the DNMMs as well as the inertia of the system, and not due to the structure of the network.

Mitigating the transmitted force due to impact can be achieved *via* reduction in the specific acoustic impedance, which is a function of the density and elastic constants of the material (eqn (3)). The pruning process reduces both the
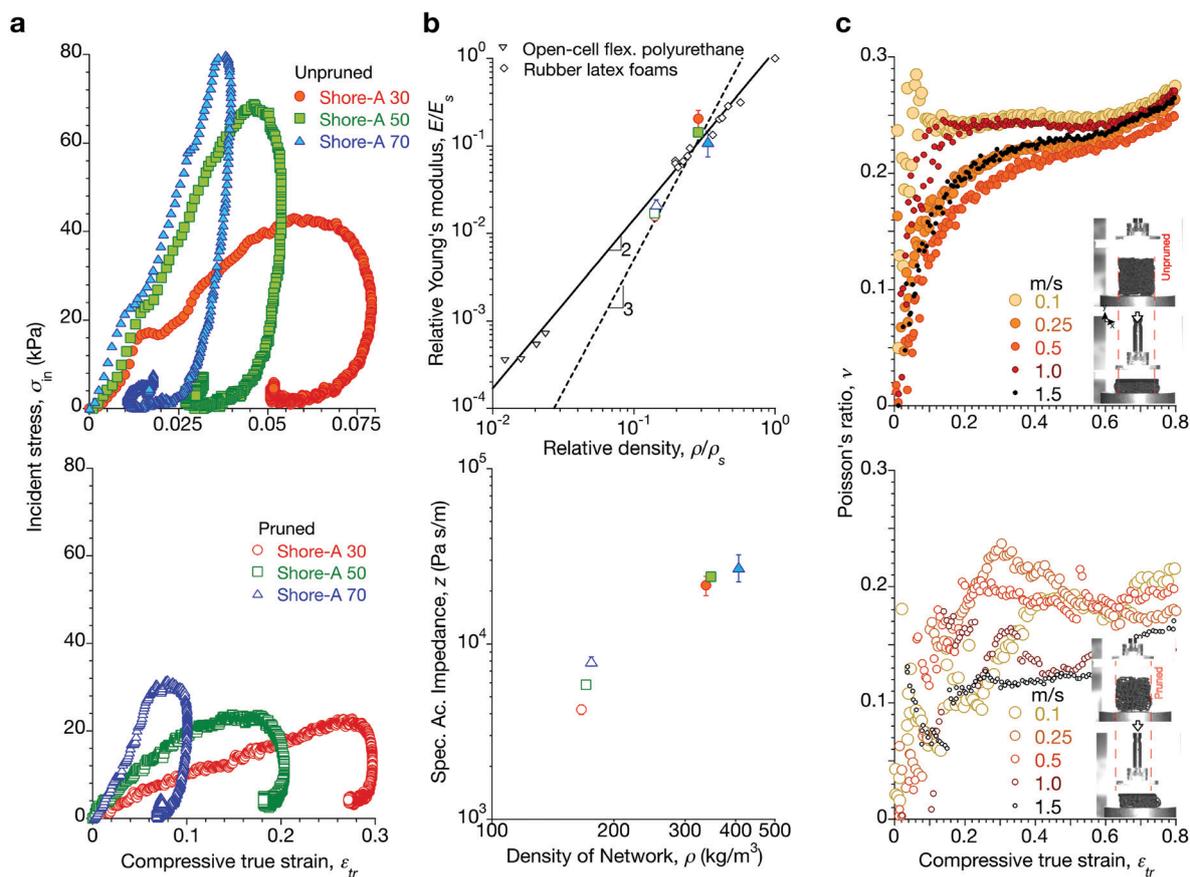

Fig. 2 Tuning the mechanical properties of DNMMs *via* pruning. (a) Dynamic impact test results showing the incident stress (σ_{in}) as a function of compressive strain (ε_{tr}) for unpruned (top plot) and pruned DNMMs (bottom plot) (b) Comparison of the DNMM Young's modulus relative to the modulus of the solid constituent material (E/E_s) (averaged over three impacts of 2.4 kg mass dropped from 50 mm height) as a function of the density of network relative to the density of the solid constituent material (ρ/ρ_s) of the unpruned and pruned DNMMs for three different printing materials (top plot). Slope of 3 and 2 are drawn as guides. A slope of 2 corresponds to the Young's modulus scaling with density in traditional open cell foams and literature data for open cell flexible polyurethane foams and rubber latex foams is shown.[12] Bottom plot shows specific acoustic impedance (z) *versus* density of network (ρ) at 0 strain of the unpruned and pruned DNMMs. (c) Poisson's ratio (ν) as a function of compressive strain (ε_{tr}) for different impact speeds of the unpruned (top plot) and pruned DNMMs (bottom plot) printed using Shore–A 30 material.

density (ρ), and elastic constants (E, K, μ) since bonds and nodes are intentionally removed from the network. This also leads to an associated change in Poisson's ratio since $\nu = f(K, \mu)$. To quantify the elastic modulus of the unpruned and pruned DNMMs (Fig. 2b), we fit the small-strain region of the stress–strain curves with a linear elastic model. Dynamic impact tests were also conducted along the three principal axes for the DNMMs (Fig. S2 and S3, ESI†). We observed no significant differences in the stress–strain behavior along the three principal axes for each network thus indicating that both the unpruned and pruned DNMMs can be assumed to be mechanically isotropic.

Fig. 2b summarizes how E and z change with ρ, and different constituent materials (with Shore-A hardness = 30, 50 and 70) for both unpruned and pruned DNMM samples. While these results are limited to this class of mechanical metamaterials, they suggest that the Young's modulus scales with the density as $E \sim \rho^n$, with $n \approx 3$. This observation is notable when comparing it to the scaling of stochastic open cell foams, where $n \approx 2$.[12] Importantly, we find there is nearly a decade reduction in E when comparing the pruned against the unpruned DNMMs. This significant reduction in the effective elastic modulus also translates to a significant change in z. We use eqn (3) and ρ at $\varepsilon_{tr} = 0$ to estimate z of the DNMMs (Fig. 2b). This result demonstrates that pruning is a rational approach for tuning the extrinsic materials properties of this class of mechanical metamaterials.

Images of the high-speed videos of the impact tests using a linear impactor illustrate the differences in the deformation in the transverse direction between the unpruned DNMM and the pruned-DNMM (inset Fig. 2c). The unpruned-DNMM expands laterally more than the pruned-DNMM when compressed indicating that the Poisson's ratio ($\nu = -\varepsilon_x/\varepsilon_y$), defined as the incremental change in the transversal (ε_x) versus the axial (ε_y) strain, of the two DNMMs are different. Fig. 2c shows that $\nu \approx 0.2$–0.35 for the unpruned DNMMs whereas the pruned DNMMs is systematically lower with $\nu \approx 0.1$–0.2. We use the values of ν and E for each sample to determine the bulk and shear moduli as a function of impact velocity. Our results show that both K and μ remain coupled for both unpruned and pruned samples (see ESI†).

The Poisson's ratio is not only strain dependent in both samples, but it also shows that the pruned DNMM displays a higher rate dependence than the unpruned DNMM. At higher impact velocities, the pruned DNMM displays a gradual decrease in the magnitude of ν that becomes more pronounced at higher compressive strains. A similar rate-dependent ν has been observed in open-cell auxetic polyurethane foams,[14] with the behavior attributed to a combination of buckling of the struts that make up the foam and inertial effects of the mechanical test. We speculate that similar effects can explain the increased rate-dependence of ν in pruned DNMM. For example, pruning can increase the effective length of the remaining bonds in the network and, therefore, change the critical conditions when buckling instabilities occur.
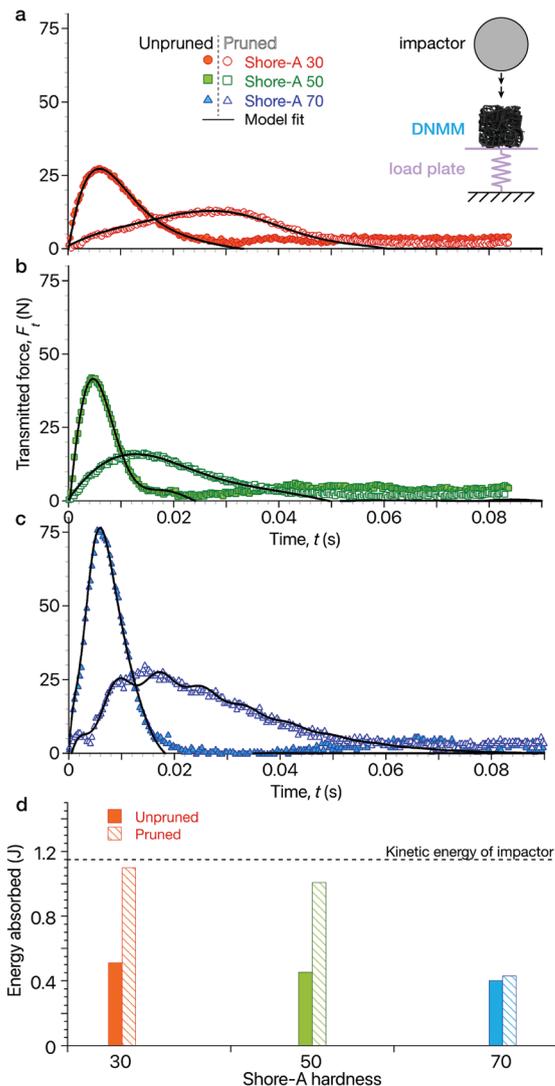

Fig. 3 Drop mass experiments of the unpruned and pruned networks. Transmitted force (F_t), measured by the force transducer beneath the DNMM, as a function of time (t) of the unpruned and pruned networks 3D printed with (a) Shore-A 30, (b) Shore-A 50 and (c) Shore-A 70. The inset figure illustrates the drop mass experiment. The change in the transmitted force is consistent with (d) the change in energy absorption of each network printed with different constituent material.

To demonstrate that pruning changes the acoustic impedance of the network, we performed drop mass experiments on the unpruned DNMM and pruned DNMM and measured the transmitted force (F_t) was using a force transducer placed underneath the sample. Fig. 3a–c compares the transmitted force (F_t) as a function of the time duration of the impact (t) of the unpruned and pruned networks for each of the constituent materials. A comparison of the first impact peaks shows that F_t is reduced for the pruned DNMMs by approximately 33% to 62% relative to that of the unpruned DNMMs. In addition to effectively reducing the magnitude of the impact, the duration of the impact event is extended, which is consistent with the notion that pruning effectively reduces the Young's modulus of

the material. We determine the amount of energy absorbed by each sample during impact by estimating the amount of mechanical work done. Fig. 3d compares the energy absorption for each of the DNMM sample compared to the kinetic energy of the impactor at the moment of impact. For each of the constitutive materials used, the pruned samples absorb more energy than the unpruned sample of the same material. The DNMM absorbs less of the impact energy as the stiffness of the constituent material increases, thus the impact energy transmitted would be higher for relatively stiffer networks. Consistent with intuition, these results suggest that increasing the compliance of the entire impact mitigation system enhances impact energy absorption but potentially at the expense of other impact mitigation parameters which we will discuss below. Nevertheless, this simple experiment demonstrates that pruning is a promising strategy for designing the next generation of materials for impact mitigation, with facile tailoring of the important materials properties.

To better understand the materials parameters that determine impact mitigation in our drop mass experiments, we modeled the results as a one dimensional mass-spring system (Fig. 1a) following an analysis similar to that of Argatov and Jokinen.[15] The resulting expression for transmitted force is defined as,

$$F_t(t) = \frac{v_0 \sqrt{\frac{k_p}{m^3}}}{\sqrt{1 - \phi^2 k_p m}} e^{-k_p \phi t} \sin\left(t \sqrt{\frac{k_p}{m}} \sqrt{1 - \phi^2 k_p m}\right) \quad (5)$$

where $\phi = \frac{c_t}{2 E_t A_t}$ and c_t is the speed of sound waves in the target, E_t is the Young's modulus of the target and A_t is the contact area between the target and the protective structure. Details on the derivation of the transmitted force model can be found in the ESI.†

Eqn (5) shows that magnitude and duration of the transmitted impulse depend on the mass of the protective material (m_p) and its stiffness (k_p). The expression successfully captures the transmitted force curves for all our experiments by linearly convoluting two ($i = 2$) waveforms of the transmitted force ($F_t(t)$). Using this expression, it is straightforward to estimate the transmitted impulse and the maximum transmitted force for any elastic material (see ESI†).

According to eqn (2), the transmitted impulse scales with the mass, or density, of the protective structure relative to that of the target. We showed in Fig. 2b that $E \sim \rho^3$ for DNMM samples, while it is widely known that traditional open cell foams scales as $E \sim \rho^2$.[12] This subtle contrast between traditional open cell foams and DNMM translates into significant differences on the effectiveness of a protective material in mitigating the transmitted impulse without making it prohibitively massive. Fig. 4a shows this dependence of the transmitted impulse on density for different $E \sim \rho^n$ relationships. Our drop mass results show that the transmitted impulse is higher for the DNMMs compared with the corresponding blocks of their respective constitutive materials (elastomer blocks). This is to be expected since impulse is related to a
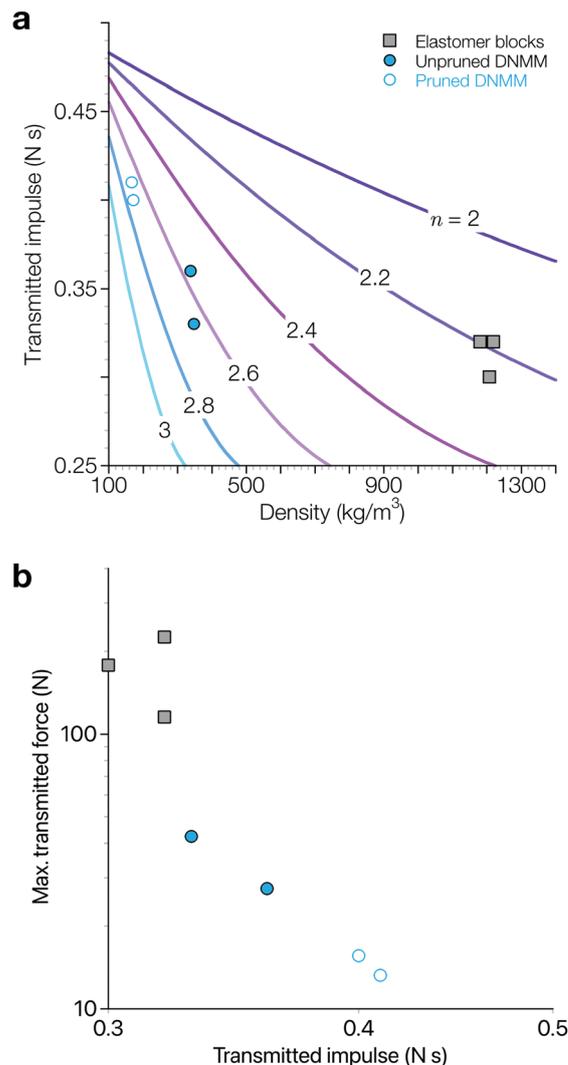

a

b

Fig. 4 (a) Transmitted impulse as a function density of protective material. Predicted trends for different $E \sim \rho^n$ relationships with scaling exponent n ranging from 2 to 3. (b) Transmitted force as a function of transmitted impulse.

change in momentum and the elastomer blocks have much higher density than the DNMMs.

An ideal impact protective material should be able to minimize both the transmitted impulse and the maximum force transmitted. Fig. 4b shows the correlation between maximum transmitted force and transmitted impulse for the DNMM materials and corresponding blocks of their respective constitutive materials. The pruning process is able to generate materials that reduce the transmitted force by almost an order of magnitude with a marginal increase in the transmitted impulse. Importantly, the pruned DNMM materials reduces both the transmitted impulse and transmitted maximum force by approximately 25% when compared with the performance, estimated using eqn (5), of a traditional open cell foam of similar density. While further optimization of the DNMMs are needed, our current results demonstrate that the pruning method is a promising new route for overcoming the transmitted force-impulse tradeoff issue found in typical impact mitigating materials.

Conclusions

There is a growing need for new materials for impact mitigation. Reaching new levels of high-performing impact mitigating materials require novel design concepts that enable development of materials that are scalable with easily tailorable material properties amenable to a wide variety of applications. Our strategy of computational design of metamaterials based on disordered networks, combined with additive manufacturing, is a promising materials-by-design approach for achieving this goal. This work represents the first experimental exploration of the mechanical response of three-dimensional disordered-network metamaterials under dynamic impact loading conditions. The experimental results presented here demonstrate that computational pruning of three-dimensional disordered networks provides a rational and flexible route to designing mechanical metamaterials with highly tunable elastic modulus and ultimate mass density. An important consequence of this pruning is the control over the specific acoustic impedance of the disordered network, which is an important property of consideration in the design of material for protective structures relevant to optimal blast/impact mitigation. This work represents an initial study of DNMM because only one disordered architecture has been explored. Future work will explore other disordered architectures and impact conditions that enable a broader range of control over ρ and E thus enabling further tunability over the materials properties relevant to impact mitigation.

Materials and methods

Certain instruments and materials are identified in this paper to adequately specify the experimental details. Such identification does not imply a recommendation by the National Institute of Standards and Technology, nor does it imply that the materials are necessarily the best available for the purpose.

Disordered networks computational details

The pruning procedure selectively removes bonds that result in the smallest reduction in the shear modulus, μ. This technique is based on the observation that in jammed networks, the change in μ_i resulting from the removal of a particular bond, μ_i, is largely independent from the change in K resulting from removing the same bond, K_i.[10,11,16] At each step in the pruning process, μ_i is calculated for each bond in the network, and the bond with the smallest value is pruned. 12.6% of nodes are removed during the pruning process, and the coordination number is reduced from 9.1 to 3.9.

Bond compressive modulus is described with a harmonic spring as discussed previously by Reid *et al.*[10] The system is relaxed at zero temperature before measurements. The elastic constants are measured similarly to techniques used previously.[10] To measure components of the shear modulus, the simulation box is deformed in such a way as to result in zero volume change to linear order. Once deformed, the system is relaxed *via* the Fire algorithm,[17] and the potential energy is measured. Examples of deformations that satisfy this criteria

include straining in the x dimension by some positive Δx and straining the y dimension by the negative.

Disordered networks printing

In order to create a model of the network for 3D printing, we use a python script that creates one bond at a time and merges them together to form the network. Each bond of the network is considered to be a cylinder with its diameter ≈ 0.4 times the average length of the bonds. The unpruned network has ≈ 2500 bonds and the pruned network has ≈ 900 bonds. We convert this structure to an STL file format that can then be 3D printed.

Disordered-Network Metamaterial samples were printed using a Stratasys Connex350 3D printer (Stratasys Ltd) using VeroWhite and TangoBlack Plus as build materials. Proprietary recipes combined the build materials to obtain the Shore-A 30, 50 and 70 hardnesses utilized as constitutive materials in the present study.

Impact testing

Constant-velocity, displacement-controlled impact tests were performed using a custom-built linear impactor. A piston driven by a computer-controlled linear actuator (Parker ETT050, Parker Hannifin Corp.) was instrumented with a dynamic force transducer (DLC101, Omega Engineering Inc.) to measure the applied force on the sample during impact. A flat acrylic plate was attached to the end of piston to evenly distribute the compressive load across (lateral dimension $\approx (100 \text{ mm})^2$) the surface of the sample. Sample deformation was captured using a high-speed camera (Phantom V12, Vision Research Inc.). The impactor plate started from rest at a height of 10 cm above the sample surface to allow the linear actuator to accelerate to the pre-set constant velocity before impact. The impactor moved with a constant velocity during impact until the pre-set displacement was reached, at which point it stopped.

Drop tower experiments were performed using a custom-built 2.4 kg drop mass equipped with a $F_{\max} = 1$ kN dynamic force transducer, dropped from a height of 50 mm onto the DNMM samples. The transmitted force was measured with force transducer plate ($F_{\max} = 22$ kN) located under the sample.

Poisson's ratio and stress–strain calculation

A custom-designed National Instruments LabVIEW edge-detection software was used to measure the changes in height ($\varepsilon_{\text{axial}}$) and average width ($\varepsilon_{\text{transverse}}$) of DNMM samples during the linear impact experiments (see ESI†). The true strain was then calculated following the definition $\varepsilon_{tr} = \ln(1 + \varepsilon_{\text{axial}})$. Impact force ($P_i$) was measured by a dynamic force transducer built into the drop mass. True stress, σ_{tr}, was estimated using the average width, w, at each strain to estimate the sample cross-sectional area in $\sigma_{tr} = P_i/w^2$.

Author contributions

M. A. R, E. P. C., C. L. S., H. M. J. and J. J. D. P. conceptualized the project. M. A. R., E. P. C., K. A. M. and E. H. performed all experiments and analyzed the data. M. A. R. and E. P. C. wrote original draft of the manuscript. DRR performed computational design of disordered networks and facilitated 3D printing of network samples. C. L. S., H. M. J. and J. J. D. P. supervised the project.

Conflicts of interest

There are no conflicts to declare.

Acknowledgements

Notes and references

1 T. Rahimzadeh, E. M. Arruda and M. D. Thouless, *J. Mech. Phys. Solids*, 2015, **85**, 98–111.
2 R. Hibbeler, *Statics and Mechanics of Materials*, Pearson Prentice Hall, 2004.
3 H. Kolsky, *J. Geophys. Res.*, 1963, **68**, 1193–1194.
4 J. Miltz and O. R. Ramon, *Polym. Eng. Sci.*, 1990, **30**, 129–133.
5 D. Satpathi, Q. Zuo, S. Donald, A. K. Maji and H. L. Schreyer, *J. Eng. Mech.*, 2002, **121**, 528–540.
6 N. J. Mills, C. Fitzgerald, A. Gilchrist and R. Verdejo, *Compos. Sci. Technol.*, 2003, **63**, 2389–2400.
7 B. J. Ramirez, U. Misra and V. Gupta, *Mech. Mater.*, 2018, **127**, 39–47.
8 A. D. Easley, M. B. B. Monroe, S. M. Hasan, A. C. Weems, J. Frederick and D. J. Maitland, *J. Appl. Polym. Sci.*, 2019, **136**, 1–9.
9 J. Christensen, M. Kadic, O. Kraft and M. Wegener, *MRS Commun.*, 2015, **5**, 453–462.
10 D. R. Reid, N. Pashine, J. M. Wozniak, H. M. Jaeger, A. J. Liu, S. R. Nagel and J. J. de Pablo, *Proc. Natl. Acad. Sci. U. S. A.*, 2018, **115**, E1384–E1390.
11 D. Hexner, A. J. Liu and S. R. Nagel, *Soft Matter*, 2018, **14**, 312–318.
12 L. J. Gibson and M. Ashby, *Proc. R. Soc. London, Ser. A*, 1982, **382**, 43–59.
13 V. Slesarenko and S. Rudykh, *Int. J. Eng. Sci.*, 2018, **123**, 62–72.
14 P. Pastorino, F. Scarpa, S. Patsias, J. R. Yates, S. J. Haake and M. Ruzzene, *Phys. Status Solidi B*, 2007, **244**, 955–965.
15 I. Argatov and M. Jokinen, *Int. J. Solids Struct.*, 2013, **50**, 3960–3966.
16 C. P. Goodrich, A. J. Liu and S. R. Nagel, *Phys. Rev. Lett.*, 2015, **114**, 1–5.
17 E. Bitzek, P. Koskinen, F. Gähler, M. Moseler and P. Gumbsch, *Phys. Rev. Lett.*, 2006, **97**, 1–4.